Sensitivity Analysis of a Coupled Hydrodynamic-Vegetation Model Using the Effectively Subsampled Quadratures Method (ESQM v5.2)

Tarandeep S. Kalra[1], Alfredo Aretxabaleta[2], Pranay Seshadri[3], Neil K. Ganju[2], and Alexis Beudin[4]

[1] Integrated Statistics, contracted to the U.S. Geological Survey, Woods Hole, MA 02543, USA
[2] U.S. Geological Survey, Woods Hole, MA 02543, USA
[3] University of Cambridge, Cambridge, England, CB2 1PZ, United Kingdom
[4] University of Bordeaux, Bordeaux, France

Correspondence to: Tarandeep S. Kalra (tkalra@usgs.gov)

Abstract. Coastal hydrodynamics can be greatly affected by the presence of submerged aquatic vegetation. The effect of vegetation has been incorporated into the Coupled-Ocean-Atmosphere-Wave-Sediment Transport (COAWST) Modeling System. The vegetation implementation includes the plant-induced three-dimensional drag, in-canopy wave-induced streaming, and the production of turbulent kinetic energy by the presence of vegetation. In this study, we evaluate the sensitivity of the flow and wave dynamics to vegetation parameters using Sobol' indices and a least squares polynomial approach referred to as Effective Quadratures method. This method reduces the number of simulations needed for evaluating Sobol' indices and provides a robust, practical, and efficient approach for the parameter sensitivity analysis. The evaluation of Sobol' indices shows that kinetic energy, turbulent kinetic energy, and water level changes are affected by plant stem density, height, and to a lesser degree, diameter. Wave dissipation is mostly dependent on the variation in plant stem density. Performing sensitivity analyses for the vegetation module in COAWST provides guidance to optimize efforts and reduce exploration of parameter space for future observational and modeling work.

1 Introduction

The presence of aquatic vegetation (e.g., mangroves, salt marshes, and seagrass meadows) provides several ecological benefits including nutrient cycling, habitat provision, and sediment stabilization (Costanza et al., 1997). Vegetation provides habitat for many species of epiphytes, invertebrates, and larval and adult fish (Heck et al., 2003). Seagrass meadows reduce sediment resuspension, thereby stabilizing bottom sediment, increasing light penetration, and improving water clarity in a positive feedback loop (Carr et al., 2010). In addition, aquatic vegetation provides coastal protection by absorbing wave energy (Wamsley et al., 2010).

30   One approach to implement the influence of aquatic vegetation on circulation is by increasing the bottom roughness

31   coefficient (Ree, 1949; Morin et al., 2000). More recently, the effect of vegetation being studied through parameterization as

32   form drag as opposed to skin friction in 2-D depth averaged models (Chen et al., 2007; Le Bouteiller and Venditti, 2015). To

33   account for 3-D vertical structures, estuary-scale models have implemented both mean and turbulent flow impacts of vegetation

34   (Temmerman et al., 2005; Kombiadou et al. 2014; Lapetina and Sheng, 2015). In addition to impacts on the flow-field, the

35   presence of vegetation also results in wave attenuation. The decay of wave height over vegetation has been simulated by

36   enhancing bed roughness (Möller et al., 1999; de Vriend, 2006; Chen et al., 2007). A more physical description of wave

37   attenuation due to vegetation was developed by Dalrymple et. al (1984), who approximated wave energy loss due to stalks

38   approximated as cylinders. This approach has been applied in spectral wave models and calibrated against flume experiment

39   results (Mendez and Lozada, 2004; Suzuki et al., 2012; Wu, 2014; Bacchi et al., 2014).

40   Recently, Beudin et al. (2017) implemented the effects of vegetation in a vertically varying water column through

41   momentum extraction and turbulence dissipation and generation using a 3D hydrodynamic model and accounting for wave

42   dissipation due to vegetation in a spectral wave model. The modeling approach was implemented and tested within the open

43   source COAWST (Coupled-Ocean-Atmospheric-Wave-Sediment Transport) modeling system that couples hydrodynamic and

44   wave models (Warner et al, 2010). The vegetation module was based on modifications to the flow field resulting from three-

45   dimensional drag, in-canopy wave-induced streaming, and production of turbulent kinetic energy in the hydrodynamics model

46   (ROMS), along with energy dissipation and resultant hydrodynamic feedback from the wave model (SWAN).

47   The vegetation module requires the user to input a given set of plant properties (stem density, height, diameter, and

48   thickness). These vegetation properties can be highly variable depending on the season and environment, yet obtaining a full

49   set of measurements in realistic settings is impractical. Identifying which properties have the greatest influence on the resulting

50   flow dynamics can reduce the amount of observational data required to robustly parameterize the model, and/or reduce the

51   number of runs required in a model ensemble to quantify the uncertainty associated with data gaps. Our study aims to perform

52   a systematic sensitivity analysis to quantify the effect of changing the vegetation properties on the resulting hydrodynamic

53   output. The results of the sensitivity analysis can be used to select and rank the most important parameters for calibration. Two

54   conditions are required for the model to display a significant sensitivity: (1) a sufficient modification of one of the forcing

55   parameters and (2) a change in the leading terms of the dynamic equations of the model. While modifying the forcing

56   parameters by a sufficient amount is required, the modification should remain within the natural range of variability of the

57   parameters.

58   Several mathematical techniques have been utilized to perform sensitivity analysis. Bryant (1987) applied scaling

59   analysis to an idealized domain and forcing and found that closure parameters such as vertical diffusivity and wind stress curl

60   were important controlling factors in thermohaline circulation. Bastidas et al. (1999) used multicriteria methods to find the

61   sensitivity of land surface scheme models that couple biosphere-atmosphere interactions. The input variables (such as

62   precipitation, air temperature and humidity etc.) predict the evolution of soil skin temperature, soil moisture, etc. The input

63   parameters obtained from the sensitivity analysis of the model showed consistency with physical properties for two different

64 field sites and helped identifying insensitive parameters that led to an improvement in model description. Fennel et al. (2001)

65 incorporated adjoint methods to perform sensitivity studies to refine ecological model parameters such that the underlining

66 model can be applied to a wider range of conditions. Mourre et al. (2008) performed multiple simulations based on realistic

67 variation of a forcing field to calculate the influence of model parameters on sea surface salinity. The metric used to measure

68 the sensitivity was based on RMS difference between the reference and modified model parameter. The results showed that

69 lateral salt diffusivity had the strongest impact on surface salinity model response. Rosero et al. (2009) investigated the

70 sensitivity of three different versions of a land satellite model (Noah LSM) applied to nine different sites based on different

71 conditions (soil, vegetation, and climate). They utilized the Monte Carlo method to generate the first order Sobol' indices

72 (Sobol', 1993), to estimate the model sensitivity. The results showed that the optimal parameter values differed varied between

73 different versions of the models and for different sites along with quantifying the nature of interactions between parameters.

74 One of the challenges associated with a Monte Carlo approach to computing the Sobol' indices is the large number of model

75 evaluations required for approximating conditional variance.

76   All these studies highlight various approaches to perform sensitivity analysis. Saltelli et al. (2008) provided a

77 comparison of different sensitivity analysis methodologies and the optimal setup for specific combinations of parameters and

78 model. Ultimately, the choice of sensitivity analysis methodology depends on multiple factors such as the computational cost

79 of running the model, the characteristics of the model (e.g., nonlinearity), the number of input parameters, and/or the potential

80 interactions between parameters. Saltelli et al. (2008) described variance-based techniques as providing the most complete and

81 general pattern of sensitivity for models with a limited number of parameters, such as the vegetation module in COAWST.

82 Sobol' indices, as a form of variance-based sensitivity analysis, provide a decomposition of the variance of a model into

83 fractions that can be assigned to inputs or combinations of inputs. However, techniques involving the estimation of Sobol'

84 indices (such as Monte Carlo methods) are expensive.

85   To reduce the computational cost and have desirable accuracy, techniques that involve approximating the global

86 response of the model with a polynomial, and then using its coefficients to estimate the Sobol' indices can be utilized (Sudret,

87 2008). In this paper, we use a set of least squares polynomial tools based on subsampling to estimate our global polynomial

88 response (Seshadri et al., 2017a). Then, the coefficients of the polynomial are used to compute the Sobol' indices. These tools

89 are implemented in the open source package Effective Quadratures Method (EQ) (Seshadri et al., 2017b), and our current work

90 provides one of the first applications of this methodology to quantify sensitivity of input parameters in coastal models.

91 Therefore, the goal of the present work is to take advantage of the EQ method to provide Sobol' indices that quantify the

92 sensitivity of the flow and wave dynamics to vegetation parameters in COAWST model. The paper is organized as follows:

93 the methods are discussed in section 2, including the numerical model with vegetation model (COAWST), Effective

94 Quadratures method to estimate Sobol' indices, and simulation design; in section 3 we present the results of sensitivity analysis

95 from various simulations; in section 4 we discuss the impact of these results; and finally in section 5 we summarize our work

96 and outline areas of future research.

97

2 Methods

2.1 COAWST implementation of vegetation model parameterization

Beudin et al. (2017) implemented a hydrodynamic-vegetation routine within the open-source COAWST numerical modeling system. The COAWST framework utilizes ROMS (Regional Ocean Modeling System) for hydrodynamics and SWAN (Simulating WAves Nearshore) for modeling waves coupled via the Model Coupling Toolkit (MCT) (Warner et al., 2008).

ROMS (Regional Ocean Modeling System) is a three-dimensional, free surface, finite-difference, terrain-following model that solves the Reynolds-Averaged Navier-Stokes equations using the hydrostatic and Boussinesq assumptions (Haidvogel et al., 2008). The transport of turbulent kinetic energy and generic length scale are computed with a generic length scale (GLS) two-equation turbulence model. SWAN (Simulating WAves Nearshore) is a third-generation spectral wave model based on the action balance equation (Booij et al., 1999). The effect of submerged aquatic vegetation in ROMS is to extract momentum, add wave-induced streaming, and generate turbulence dissipation. Similarly, the wave dissipation due to vegetation modifies the source term of the action balance equation in SWAN. Sub-grid scale parameterizations account for changes due to vegetation in the water column extending from the bottom layer to the height of the vegetation in the flow model, while SWAN accounts for wave dissipation due to vegetation at the seafloor. The parameterization of SWAN to account for wave dissipation implemented by Suzuki et al. 2012 has the same effect as energy dissipation.

The parameterizations used to implement the effect of vegetation in both ROMS and SWAN models are mentioned in Table 1 and detailed in Beudin et al. (2017). The coupling between the two models occurs with an exchange of water level and depth averaged velocities from ROMS to SWAN and wave fields from SWAN to ROMS after a fixed number of time steps (Fig. 1). The vegetation properties are separately input in the two models at the beginning of the simulations.

2.2 Method for Sensitivity Analysis: Polynomial Least Squares

Polynomial techniques are ubiquitous in the field of uncertainty quantification and model approximation. They estimate the response of some quantity of interest with respect to various input parameters using a global polynomial. From the coefficients of the polynomial the mean, variance, skewness, and higher order statistical moments can be calculated (see Smith 2014; Geraci et al. 2016). In this paper, our interest lies in statistical sensitivity metrics called first order Sobol' indices (Sobol', 1993) that are derived from the conditional variances of the parameters of the model. These indices are the same in number as the input parameters to the model and quantitatively rank the input parameters based on their contribution to the resultant model output. Thus, model output is more sensitive to parameters that exhibit higher first order Sobol' index value. Second order and third order Sobol' indices may also be computed. The sum of the first, second, and third order Sobol' indices should sum to unity, therefore if the first order indices are themselves close to unity, it indicates the higher order interaction between model input parameters is weak.

4

130   In this paper, the first order indices are computed from a global polynomial model using Effectively Subsampled
131 Quadratures Method (ESQM v5.2; Seshadri et al., 2017b). There are two attributes to any data-driven polynomial model: the
132 choice of the polynomial basis and the strategy for estimating the coefficients of the polynomial. The basis used in Effective
133 Quadratures are orthogonal polynomials; i.e. orthogonal with respect to the weight of the input parameter. For example, if one
134 of the input parameters is prescribed with a Gaussian distribution, then a Hermite orthogonal polynomial basis would be used;
135 likewise for a uniform distribution, Legendre polynomials are used. In the current work, a uniform distribution is assumed for
136 the input parameter space. The rationale behind selecting polynomials that are orthogonal with respect to the input weight is
137 that it reduces the number of model evaluations required for estimating statistical moments. Details on the exponential
138 convergence in moments when matching the orthogonal polynomial with its corresponding weight can be found in Xiu et al.
139 (2002).

140   The coefficients for the polynomial expansion are typically approximated using an integral over the input parameter
141 space using quadrature rules. When the number of input parameters is greater than one, tensor grid or sparse grid based
142 quadrature rules may be used to approximate these integrals. However, the cost of tensor grids grows exponentially with
143 dimension, i.e., a four-point quadrature rule in three dimensions has 5^3 points, in four dimensions has 5^4 points and so on.
144 While some alleviation can be obtained using sparse grids, in this paper a more efficient sampling technique is used: effectively
145 subsampled quadratures (abbreviated to Effective Quadratures).

146   The method of Effective Quadratures determines points for approximating the integral by subsampling well-chosen
147 points from a tensor grid, and evaluating the model at those subsamples. These well-chosen points are obtained via a QR
148 column pivoting heuristic (Seshadri et al. 2017a). Once the coefficients are estimated, the Sobol' indices can be readily
149 computed (Sudret 2008).

150

151 **2.3 Range of input vegetation properties for sensitivity analysis**
152 Prior to performing the simulations for estimating Sobol' indices described above, a range of vegetation inputs that would
153 impact the model response needs to be chosen. Kennish et al. (2013) constrained annual variation of three of the four vegetation
154 properties (stem density, height, diameter) based on *Zostera marina* growth in the Barnegat Bay-Little Egg Harbor estuary.
155 The thickness of *Z. Marina* is selected to be an order of magnitude lesser than its diameter based on Lakrum et al., 2007. Based
156 on this, the range of the vegetation model inputs evaluated is as follows:
157   1.   Stem density (n_v)= [38.2 - 250.4] stems/m^2.
158   2.   Height (l_v) = [0.16 – 0.32] m.
159   3.   Diameter (b_v) = [1.0 – 10.0] mm.
160   4.   Thickness (t_v) = [0.1 – 1.0] mm.
161 For the sensitivity analysis, a combination of these ranges of inputs (Table 2) is chosen to configure different simulations in
162 an idealized test case, described below. In addition to these four vegetation properties, the vegetative model requires an input
163 of drag coefficient (C_D) in the flow model and the wave model. However, variations on C_D are unlikely to be measured in the

164 field and thus users could rely on the published literature for an appropriate choice based on the type, shape, and flexibility of
165 the vegetation under study.

166

2.4 Test case configuration

168 An idealized rectangular model domain of 10 km by 10 km with a 3 m deep basin is chosen. The grid is 100 by 100 in the
169 horizontal (100 m resolution) and has 60 vertical sigma-layers (uniformly distributed) leading to 0.05 m resolution in the
170 vertical. The vertical resolution of 0.05 m allows a plant height of 0.27 m to be distributed over 6 vertical layers while the
171 shortest height is restricted to 2 vertical layers. A square patch of vegetation (1 km by 1 km) is placed in the middle of the
172 domain. The ROMS barotropic and baroclinic time steps are respectively *0.05 s and 1 s*, while the SWAN time step and the
173 coupling interval between ROMS and SWAN are 10 min. The friction exerted on the flow by the bed is calculated using the
174 SSW bbl in the bottom boundary layer formulation (Warner et al., 2008). The bottom boundary layer roughness is increased
175 by the presence of waves that produce enhanced drag on the mean flow (Madsen, 1994; Ganju and Sherwood, 2010). The
176 vegetative drag coefficients (C_D) in the flow model and the wave model are set to 1 (typical value for a cylinder at high
177 Reynolds number). The bed roughness is set to z_0=0.05 mm, which corresponds to a mixture of silt and sand (Soulsby, 1997).
178 The turbulence model selected is the $k - \varepsilon$ scheme (Rodi, 1984).

179 The model is forced by oscillating the water level on the northern edge with a tidal amplitude of 0.5 m and a period
180 of 12 h. Waves are also imposed on the northern edge with a height of 0.5 m, directed to the south (zero angle), with a period
181 of 2 s. The test case setup is similar to the one used by Beudin et al., (2017). The test case setup is simulated for 2 days to
182 obtain a tidally steady state solution. These simulations require 40 CPU hours on Intel Xeon(R) X5650 2.67 GHz processors
183 running on 24 parallel processors.

184

2.5 Choice of COAWST model response to vegetation inputs

186 The output parameters used to investigate the vegetation model sensitivity are chosen to reflect the first order effects of
187 vegetation on the hydrodynamics and waves. The results for the model response are computed for the last tidal cycle (a total
188 of 3 tidal cycles are required for achieving steady state). The presence of vegetation affects the output parameters in different
189 physical ways (Table 1) as:
190 1. Wave energy dissipation: Vegetation dissipates wave energy by reducing wave height, increasing wavelength, and reducing
191 wave steepness.
192 2. Kinetic energy: A drag force is generated by plants. This leads to a decrease in kinetic energy within and behind the
193 vegetation patch.
194 3. Water level: As the wave energy (and momentum) flux decreases due to bottom friction, the mean water level increases to
195 balance the decrease in wave and kinetic energy. The flow decelerates in front of the patch and in the wake of the patch while
196 it accelerates around the edges of the patch, leading to a water level gradient.

197 4. Turbulent kinetic energy (TKE): Reduced turbulent kinetic energy in front and within the patch. The enhancement of TKE

198 inside the boundary layer is not captured with the current resolution.

199 The response impact to change in the inputs during each simulation is computed by calculating the percentage

200 difference of model response for each simulation from the minimum value of all the simulations. The model response is

201 obtained in and around the vegetation patch and averaged over the last tidal cycle. The change in model response of water

202 level is computed by finding the maximum water level difference in and around the vegetation patch. In addition, the variability

203 of model response with given vegetation inputs in different simulations is calculated through standard deviation of model

204 response in and around the vegetation patch over the last tidal cycle. The standard deviation in TKE is depth averaged to

205 provide a 2-D field.

206

207 **3 Results**

208 **3.1 Setting up simulations with different vegetation inputs**

209 Using the range of input parameters described above (section 2.3), and assuming all the inputs are uniformly distributed over

210 their ranges, a matrix of design of experiment values (Table 2) was determined using Effective Quadratures. A total of 15

211 simulations were found to be required, corresponding to the number of coefficients in a 4D polynomial with a maximum order

212 of 2. In general, the number of coefficients n, is given by the formula

213
$$n = \binom{d + o}{d},$$

214 where d is the number of dimensions and o is the maximum order (assuming it is isotropic across all dimensions).

215

216 **3.2 Model response from all the simulations**

217 The 15 simulations (parameter choice of each simulation in Table 2) are performed to provide model response from the four

218 chosen output variables.

219 1. Wave dissipation: The percentage change in wave dissipation from all simulations relative to the minimum value of wave

220 dissipation varied between 75 and 600% (Fig. 3(a)). Simulation 2, which includes the combination of smallest stem density

221 (n_v= 62.1 stems/m^2) and shortest height (0.174m), incurred the least wave dissipation, while simulation 3, which involved the

222 combination of greatest stem density (n_v= 226.5 stems/m^2) and tallest height (0.295 m), resulted in greatest wave dissipation.

223 The greatest amount of variability in wave dissipation occurs in front of the vegetation patch (Fig. 4), where the greatest

224 amount of wave energy is dissipated due to the presence of the vegetation patch.

225 2. Kinetic energy: The percentage change in kinetic energy from all simulations relative to the minimum kinetic energy varied

226 between 5.0 and 34.0 % (Fig. 3b). Simulation 8, performed with an intermediate value of stem density along with the largest

227 values of height, diameter, and thickness, results in the least amount of kinetic energy (lowest velocities). Simulation 2 causes

228 the least amount of extraction of momentum with a combination of smallest plant stem density, height, and diameter values,

229 resulting in the greatest kinetic energy in and around the vegetation patch. The variability in kinetic energy from all the

simulations is observed at a cross section along the vegetation patch (Fig. 5). Variability is observed throughout the water column where the vegetation patch exists. Similar to the variability in wave dissipation, the greatest amount of variability occurs in front of the vegetation patch. The region of maximum variability occurs at a distance of (0.25 − 1.25) m above bed.

3. Water level: The percentage change in maximum water level difference from all simulations relative to the minimum of the maximum water level difference varied between 3.0 and 18.0 % (Fig. 3c). The minimum water level gradient is obtained from simulation 13 that includes a combination of plant inputs (n_v = 62.1 stems/m^2 (minimum), l_v = 0.174 m (intermediate), diameter=6 mm (minimum), and t_v = 0.3 mm (minimum). Simulations 2, 6, and 11 also give relatively low values of water level gradient. Simulations 2 and 6 both involve the smallest plant stem density values (i.e. n_v = 62.1 stems/m^2). On the other hand, simulation 8 (n_v=144.3 stems/m^2, l_v = 0.3 m (maximum),b_v=9 mm, and t_v = 0.9 mm) accounts for the greatest value of maximum water level difference. The variability in water level (Fig. 6) is highest around the lobes of the vegetation patch where the water level adjusts owing to changes in velocity around the patch. Behind the vegetation patch, the variability increases as the water level adjusts to the change in flow conditions.

4. Turbulent Kinetic Energy (TKE): The percentage change in TKE from all simulations relative to the minimum TKE varied between 0.5 and 10.0 % (Fig. 3d). Simulation 8 (combination of plant n_v = 144.3 stems/m^2, l_v = 0.3 m, b_v = 9 mm and t_v = 0.9 mm) gives the greatest amount of TKE, similar to what was observed with kinetic energy change. The smallest value of TKE is obtained in and around the vegetation patch in simulation 2 with a combination of plant inputs (n_v = 62.1 stems/m^2, l_v = 0.2 m, b_v = 3 mm, and t_v = 0.6 mm). Simulation 2 causes the least amount of dissipation of turbulence with a combination of smallest plant stem density, height and diameter. The variability in TKE peaks occurs in front of the vegetation patch (Fig. 7) where the different simulations dissipate turbulence to substantially different degrees. The changes in turbulence mixing caused by the presence of the vegetation patch are close to zero inside the patch (all simulations dissipate similar amounts of turbulence).

3.3 Quantifying sensitivity using Sobol' Indices

Following the variability in model response from different simulations, the sensitivity to input vegetation parameters can be quantified with the use of first order Sobol' indices that are obtained by taking advantage of the Effective Quadratures approach. Sobol' indices are individually computed for all the model responses. The first order Sobol' indices for all the model responses (Table 3) add up to more than 0.9. This results indicates they account for 90% of the variability in model response for the given vegetation property inputs, and the variability captured by second order and third order indices is relatively low. The model is most sensitive (Table 3) to plant stem density (n_v) and height (l_v) over the range of parameters considered; these two inputs account for over 80% of the sensitivity to all model outputs. The vegetation diameter (b_v) accounts for 12-15 % of model sensitivity to kinetic energy, water level change, and turbulent kinetic energy. Thickness (t_v) showed the least impact on all the chosen model outputs.

4 Discussion

4.1 Variability in model response from sensitivity analysis

From the different simulations performed during sensitivity analysis, there is a great amount of variability in front of the vegetation patch in wave dissipation, KE, and TKE (Figs. 4, 5 and 7). This is a result of large amount of wave dissipation and flow deceleration in front of the vegetation patch. The cross-sectional plane of the domain illustrates that the variability in KE occurs throughout the water column (Fig. 5), highlighting the 3-D impact of vegetation inputs. Interestingly, the greatest amount of variability in KE (Fig. 5) occurs at distance above the bed between $0.4 - 1.3$ m at y = 5.6 km, while the maximum vegetation height in all the simulations is 0.3 m. This result indicates that variation in vegetation height results in the greatest amount of KE variability above the vegetation patch. The variability in water level change is large around the lobes and behind the vegetation patch (Fig. 6). The variability in these regions is because the change in local flow velocity is adjusted by a change in water level around the vegetation patch. This is further confirmed by observing the variation in velocity profiles with depth (Fig. 8a) at a particular time instance during flood tide. Simulation 8 results in the lowest velocity of 0.06 m/s while simulation 2 results in the peak flood velocity of 0.11 m/s. Consequently, the gradient of velocity with respect to depth is greatest at all depths for simulation 8 while least for simulation 2 (Fig. 8b). The gradient reaches a maximum value at the bottom layer.

4.2 Understanding vegetation parameterization to interpret Sobol' Indices

The parameterizations involving extraction of momentum, turbulence production, and turbulence dissipation are directly affected by vegetation stem density (n_v), diameter (b_v), and thickness (t_v) (Table 1). Because these mechanistic processes occur at the blade scale, the dependence on vegetation height (l_v) is implicitly included in the parameterizations. Sobol' indices provide quantifiable information and show that vegetation height, stem density, and diameter (in decreasing order of importance) are pertinent in accurately computing kinetic energy (KE), turbulent kinetic energy (TKE), and water level. An accurate representation of KE and TKE has direct ramifications on estimating sediment transport while water level estimates can affect storm surge predictions.

The high sensitivity of wave dissipation to vegetation stem density highlights the need of accurate density representation to attain wave attenuation estimates, especially in open coasts. SWAN computes wave dissipation due to vegetation as a bottom layer effect. Therefore, the height of the vegetation does not affect wave dissipation to the same extent as other model outputs: KE, TKE, and water level. In addition, the equation representing the wave dissipation process in SWAN is independent of vegetation thickness, thus corresponding to the lowest Sobol' index. Vegetation thickness only appears in the turbulence dissipation term (Table 1) modifying the turbulence length scale has the least effect on any of the model responses.

4.3 Linear curve fitting to complement Effective Quadratures based sensitivity analysis

297   To complement the results of the Sobol' indices calculation, linear fits to the data are conducted. The main parameter
298   contributing to the wave dissipation variability is the stem density explaining over 80% of the variability (R^2=0.81). The least
299   squared fit to wave dissipation that included all parameters combined explains 98% of the variability. When fitting models, it
300   is possible to increase the explained variance by using more complex fitting models adding parameters, but doing so may result
301   in over-fitting. The Bayesian Information Criterion (BIC; Schwarz, 1978; Aretxabaleta and Smith, 2011) provides a non-
302   subjective metric for the best fit by penalizing over-parameterization. BIC resolves over-fitting by introducing a penalty term
303   for the number of parameters in the model. For wave dissipation, the BIC approach identified a fit based exclusively on density
304   as the model that best match the data while preventing over-fitting. The selection of density as the single most relevant
305   parameter is consistent with the Sobol' indices result (Table 3).

306   The kinetic energy variability is also associated with stem density changes, but the percentage of explained variability
307   (42%) is smaller than for wave dissipation. Diameter and height also contributed to changes in kinetic energy. The combination
308   of stem density, height, and diameter provided the optimal fit of the data (selected by minimizing BIC) and explained 89% of
309   variability in kinetic energy. Similar results were obtained for TKE with density explaining 45% of the variability but the
310   combination of stem density, height, and diameter providing the optimal fit to TKE (selected by minimizing BIC) and
311   explained 87% of the variability. The model response of water level variability is also best explained by a combination of stem
312   density, height, and diameter (96% of water level variance explained). Thickness was not correlated with wave dissipation,
313   kinetic energy or TKE and only contributed to water level gradient variability.

314

315   **4.4 Limitations of the current sensitivity methodology**

316   The model configuration chosen includes vegetation covering a small fraction of the water column to allow for proper wave
317   dissipation. Many species of seagrass have a larger vertical footprint and can also exhibit much higher shoot densities. The
318   goal of the study is to provide estimates on the relative importance of the different parameters through a robust sensitivity
319   approach. The current work assumed rigid vegetation blades, while the model is capable of including flexible vegetation by
320   altering the blade scale. The expected effect of flexible blades would be to reduce the relative importance of vegetation length
321   (l_v) on the model outputs. In addition, the present work assumes a constant drag coefficient for cylindrical vegetation shape;
322   the influence of a variability drag coefficient can be a subject of a future sensitivity study. Other model parameters such as
323   vertical and horizontal resolution, mixing parameterization, and wave and hydrodynamic forcings will also affect model
324   results, but were beyond the scope of the current study.

325   **5 Conclusions**

326   The coupled wave-flow-vegetation module in the COAWST modeling system provides a tool to study vegetated flows in
327   riverine, lacustrine, estuarine, and coastal environments. The resulting flow field in the presence of vegetation depends on its
328   properties, including vegetation stem density, height, diameter, and thickness. The sensitivity of the hydrodynamic and wave
329   conditions to changes in vegetation parameters is investigated. The sensitivity analysis helps in understanding the

10

multiparameter/multiresponse of various interactions within the model. We use an existing tool that formulates the Effective Quadratures method to quantify the sensitivity of plant input properties for the vegetation module in COAWST model. The decomposition of the variance of the model solution given by the Sobol' indices is assigned to plant parameters.

The method of using Sobol' indices to quantify sensitivity can be computationally expensive. One of the goals of this work is to demonstrate a robust, practical, and efficient approach for the parameter sensitivity analysis. We show that the approach of using Effective Quadratures method to select a parameter space that is consistent with physical understanding significantly reduces the computational time required to obtain the Sobol' indices.

The evaluation of Sobol' indices shows that the input values of plant stem density, height and to a lesser degree, diameter are consequential in determining kinetic energy, turbulent kinetic energy and water level changes. Meanwhile, the wave dissipation is mostly dependent on the variation in plant density.

The sensitivity analysis for the vegetation model in COAWST presented herein provides guidance for observational and modelling work by allowing future efforts to focus on constraining the most influential inputs without having to explore the entire parameter space. An accurate representation of processes causing kinetic energy and turbulent kinetic energy leads to enhanced understanding of sediment processes while accurate water level computations help to predict coastal flooding caused by storm surge. Similarly, wave attenuation measurements in open coasts are better understood with a correct representation of wave dissipation. In the future, we intend to perform a similar sensitivity analysis with the inclusion of a biological model that will affect plant growth, thus allowing a time dependence of model input and response. In addition, the influence of vegetation on sediment transport will be explored. As model complexity increases with more parameters representing additional processes, input parameter sensitivity is required for the model to be applied on practical applications.

6 Code availability

The Effective Quadratures methodology is an open source Python based tool designed to perform sensitivity analysis for a given physical system. The instructions to install the code along with all the open source files for this tool are detailed here: https://github.com/Effective-Quadratures/Effective-Quadratures. For any further inquiries about the Effective Quadratures methodology, please contact the corresponding author Dr. P. Seshadri (ps583@cam.ac.uk).

The COAWST model is an open source coupled hydrodynamics and wave model containing vegetation effects mainly coded in Fortran 77. This model provided the physical setting to perform the sensitivity analysis. The code is available from https://coawstmodel-trac.sourcerepo.com/coawstmodel_COAWST after registration via email with J. C. Warner (jcwarner@usgs.gov).

7 Data availability

The model output from various simulations used to perform sensitivity analysis in this study are available at: http://geoport.whoi.edu/thredds/catalog/clay/usgs/users/tkalra/senstivity_study/catalog.html. The link contains a "README.txt" file that explains how the folder is organized to contain model output.

364

8 Author contribution

T. S. Kalra, and N. K. Ganju designed and simulated the numerical experiment space for sensitivity analysis. P. Seshadri developed the Effective Quadratures methodology to quantify the model sensitivity. A. Beudin provided inputs on the mechanistic processes involving the vegetation model. T. S. Kalra and A. Arextabaleta performed the data analysis from the output of sensitivity study and prepared the manuscript with contributions from all co-authors.

370

9 Disclaimer

Any use of trade, firm, or product names is for descriptive purposes only and does not imply endorsement by the U.S. Government.

374

10 Acknowledgement

We thank Jeremy Testa at University of Maryland Center for Environmental Science for providing us guidance on the ranges of vegetation for sensitivity studies in the early stages of work. We also thank you P. Soupy Daylander at U. S. Geological Survey, St. Petersburg Coastal and Marine Science Center for providing her feedback to improve the clarity of the paper. We thank the anonymous reviewers for their careful reading of our manuscript and their insightful comments and suggestions.

380

11 References

Aretxabaleta A.L., Smith K.W.: Analyzing state-dependent model-data comparison in multi-regime systems, Computers & Geosciences, 15, 627–636, 2011.

Baptiste M., Ballabrera-Poy J., García-Ladona E., and Font, J.: Surface salinity response to changes in the model parameters and forcings in a climatological simulation of the eastern North-Atlantic Ocean, Ocean Modeling, 23, 21-32, 2008.

Bastidas, L. A., Gupta, H. V., Sorooshian, S., Shuttleworth, W. J., and Yang, Z. L.: Sensitivity analysis of land surface scheme using multicriteria methods, Journal of Geophysical Research, 104, 481-490, 1999.

Beudin, A., Kalra, T. S., Ganju, N., K., and Warner, J.C.: Development of a Coupled Wave-Current-Vegetation Interaction, Computers & Geosciences, 100, 76-86, 2017.

Bryan, F.: Parameter Sensitivity of Primitive Equation Ocean General circulation models, Journal of Physical oceanography, 17, 970-985, 1986.

Booij, N., Ris, R. C., and Holthuijsen, L. H.: A third-generation wave model for coastal regions, Part I, Model description and validation, Journal of Geophysical Research C4, 104, 7649-7666, 1999.

Carr, J., D'Odorico P., McGlathery K., and Wiberg, P.: Stability and bistability of seagrass ecosystems in shallow coastal lagoons: role of feedbacks with sediment resuspension and light attenuation, Journal of Geophysical Research, 115, G03011, 2010.

Chen, S. N., Sanford L., Koch E. W., Shi F., and North, E. W.: A nearshore model to investigate the effects of seagrass bed

398 geometry on wave attenuation and suspended sediment transport, Estuaries and Coasts, 30(2), 296-310, 2007.

399 Costanza, R., d'Arge, R., de Groot, R., Farberk, S., Grasso, M., Hannon, B., Limburg, K., Naeem, S., O'Neill, R.V., Paruelo,

400 J., and Raskin, R.G.: The value of the world's ecosystem services and natural capital, Nature 387, 253-260, 1997.

401 Dalrymple, R. A., Kirby, J. T., and Hwang, P. A.: Wave diffraction due to areas of energy dissipation. Journal of Waterway,

402 Port, Coastal, and Ocean Engineering, 110, 67-79, 1984.

403 de Vriend, H. J.: Integrated research results on hydrobiosedimentary processes in estuaries: algorithm for vegetation friction

404 factor, Defra R&D Technical Report FD1905/TR3, 2006.

405 Fennel, K., Losch, M., Schroter, J., and Wenzel, M.: Testing a marine ecosystem model: sensitivity analysis and parameter

406 optimization, Journal of Marine Systems, 28, 45–63, 2000.

407 Geraci, G., Congedo, P. M., Abgrall, R., and Iaccarino, G.: High-order statistics in global sensitivity analysis: Decomposition

408 and model reduction. Computer Methods in Applied Mechanics and Engineering, *301*, 80-115, 2016.

409 Heck, K.L., Hays, G. and Orth, R.J.: Critical evaluation of the nursery role hypothesis for seagrass meadows, Marine Ecology

410 Progress Series, 253, 123-136, 2003.

411 Hemming, M. A., and Duarte, C. M.: Seagrass Ecology, Cambridge, UK: Cambridge University Press, 2000.

412 Lapetina A., and Sheng, Y. P.: Three-dimensional modeling of storm surge and inundation including the effects of coastal

413 vegetation, Estuaries and Coasts, 37, 1028-1040, 2014.

414 Larkum, A. W. D, Orth, R. J., and Duarte, C. M.: In Seagrasses: Biology, Ecology and Conservation, Springer Netherlands,

415 2007.

416 Luhar M., Coutu S., Infantes E., Fox S., and Nepf H. M.: Wave-induced velocities inside a model seagrass bed, Journal of

417 Geophysical Research, 115, C12005, 2010.

418 Luhar, M., and Nepf, H. M.: Flow-induced reconfiguration of buoyant and flexible aquatic vegetation. Limnology and

419 Oceanography, 56(6), 2003-2017, 2011.

420 Luhar, M., and Nepf, H. M.: Wave-induced dynamics of flexible blades. Journal of Fluids and Structures, 61, 20-41, 2016. Le

421 Bouteiller, C., and Venditti, J. G.: Sediment transport and shear stress partitioning in a vegetated flow. Water Resources

422 Research, 51, 2901-2922, 2014.

423 Madsen, O.S.: Spectral wave–current bottom boundary layer flows. Proceedings of the 24th International Conference on

424 Coastal Engineering Research Council, Kobe, Japan, 384-398, 1994.

425 Marjoribanks, T. I., Hardy, R. J., and Lane, S. N.: The hydraulic description of vegetated river channels: the weaknesses of

426 existing formulations and emerging alternatives, WIREs Water, 1, 549-560, 2014.

427 Mendez, F. M., and Losada, I. J.: An empirical model to estimate the propagation of random breaking and nonbreaking waves

428 over vegetation fields, Coastal Engineering, 51, 103-118, 2004.

429 Möller, I., Spencer, T., French, J. R., Legget, D. J., and Dixon, M.: Wave transformation over salt marshes: a field and numerical

430 modeling study from Norfolk, England. Estuarine, Coastal and Shelf Science, 49, 411-426, 1999.

431 Morin, J., Leclerc, M., Secretan, Y., and Boudreau, P.: Integrated two-dimensional macrophytes-hydrodynamic modelling,

432 Journal of Hydraulic Research, 38, 163-172, 2000.

433 Morison, J. R., O'Brien, M. P., Johnson, J. W., and Schaaf, S. A.: The force exerted by surface waves on piles, Petroleum
434 Transactions, AIME, 189, 149-154.

435 Mourre, B., Ballabrera-Poy, J., García-Ladona, E., Font, J.: Surface salinity response to changes in the model parameters and
436 forcings in a climatological simulation of the eastern North-Atlantic Ocean, Ocean Modeling, 23, 37-49, 2008.

437 Kennish, M. J., Fertig, M. B., and Sakowicz, G. P.: In situ Surveys of Seagrass Habitat in the Northern Segment of the Barnegat
438 Bay-Little Egg Harbor Estuary, Barnegat Bay Partnership, Final Report, 2013.

439 Kombiadou, K., Ganthy, F., Verney, R., Plus, M., and Sottolichio, A.: Modelling the effects of Zostera noltei meadows on
440 sediment dynamics: application to the Arcachon lagoon, Ocean Dynamics, 64, 1499-1516, 2014.

441 Ree, W. O.: Hydraulic characteristics of vegetation for vegetated waterways, Agricultural Engineering, 30, 184-189, 1949.

442 Saltelli, A., Ratto, M., Andres, T., Campolongo, F., Cariboni, J., Gatelli, D., Saisana, M., and Tarantola, S.: Global sensitivity
443 analysis: the primer, John Wiley & Sons, Chichester, 312 pp, 2008.

444 Rodi, W.: Turbulence models and their application in hydraulics, a state of the art review. Technical report, International
445 Association of Hydraulics Research, Delft, 1984.

446 Rosero, E., Yang, Z. L., Wagener, T., Gulden, L. E., Yatheendradas, S., and Niu, G. Y.: Quantifying parameter sensitivity,
447 interaction, and transferability in hydrologically enhanced versions of the Noah land surface model over transition zones during
448 the warm season, Journal of Geophysical Research 115, 2010.

449 Seshadri, P., Narayan, A., and Mahadevan, S.: Effectively Subsampled Quadratures for Least Squares Polynomial
450 Approximations, arXiv: 1601.05470, 2017a.

451 Seshadri, P., Parks, G. T.: Effective Quadratures (EQ): Polynomials for Computational Engineering Studies, Journal of Open
452 Source Software, 2(11), DOI: 10.21105/joss.00166, 2017b.

453 Sheng, Y. P., Lapetina, A., and Ma, G.: The reduction of storm surge by vegetation canopies: three-dimensional simulations,
454 Journal of Geophysical Research, 39, L20601, 2012.

455 Smith, R. C.: Uncertainty quantification: theory, implementation, and applications, Vol. 12. SIAM, 2013.

456 Soulsby, R. L.: Dynamics of Marine Sands, Thomas Telford, London, 249 pp, 1997.

457 Sobol', Ilya. M.: Sensitivity estimates for nonlinear mathematical models, Mathematical Modelling and Computational
458 Experiments, 1.4, 407-414, 1993.

459 Sudret, B.: Global sensitivity analyzing using polynomial chaos expansions, Reliability Engineering and System Safety, 93,
460 pp. 964-979, 2008.

461 Suzuki T., Zijlema, M., Burger, B., Meijer, M. C., and Narayan, S., Wave dissipation by vegetation with layer schematization
462 in SWAN, Coastal Engineering, 59(1): 64-71, 2012.

463 Temmerman, S., Bouma, T. J., Govers, G., Wang, Z. B., De Vries, M. B., and Herman, P. M. J.: Impact of vegetation on flow
464 routing and sedimentation patterns: three-dimensional modeling for a tidal marsh, Journal of Geophysical Research, 110,
465 F04019, 2005.

466 Uittenbogaard, R.: Modelling turbulence in vegetated aquatic flows, International workshop on Riparian Forest vegetated
467 channels: hydraulic, morphological and ecological aspects, Trento, Italy, 2003.

468 Umlauf, L., and Burchard, H.: A generic length-scale equation for geophysical turbulence models, Journal of Marine Research,
469 61, 235-265, 2003.

470 Van Katwijk, M. M., Bos, A.R., Hermus, D. C. R., and Suykerbuyk, W.: Sediment modification by seagrass beds: muddification
471 and sandification induced by plants cover and environmental conditions, Estuarine, Coastal and Shelf Science, 89, 175-181,
472 2010.

473 Wamsley, T.V., Cialone, M.A., Smith, J.M., Atkinson, J.H. and Rosati, J.D.: The potential of wetlands in reducing storm surge,
474 Ocean Engineering, 37(1), 59-68, 2010.

475 Warner, J. C., Sherwood, C. R., Arango, H. G., and Signell, R. P.: Performance of four turbulence closure models implemented
476 using a generic length scale method, Ocean Modelling, 8, 81-113, 2005.

477 Warner J. C., Sherwood, C. R., Signell, R. P., Harris, C. K., and Arango, H.G.: Development of a three-dimensional, regional,
478 coupled wave, current, and sediment-transport model, Computer & Geosciences, 34, 1284-1306, 2008.

479 Warner, J. C., Perlin, N., and Skyllingstad, E. D.: Using the Model Coupling Toolkit to couple earth system models,
480 Environmental Modelling & Software, 23, 1240-1249, 2008.

481 Warner, J. C., Armstrong, B., He, R., and Zambon, J. B.: Development of a Coupled Ocean-Atmosphere-Wave-Sediment
482 Transport (COAWST) Modeling System, Ocean Modelling, 35, 230-244, 2010.

483 Warner, J. C., Defne, Z., Haas, K., and Arango, H. G.: A wetting and drying scheme for ROMS, Computer & Geosciences, 58,
484 54-61, 2013.

485 Wu, W.: A 3-D phase-averaged model for shallow-water flow with waves in vegetated water, Ocean Dynamics, 64, 1061-1071,
486 2014.
487
488
489
490
491
492
493
494
495
496
497
498
499

Process	Equation	n_v	l_v	b_v	t_v
Extraction of Momentum	$$F_{d,veg,u} = \frac{1}{2} C_D b_v n_v u \sqrt{u^2 + v^2}$$ C_D = Plant drag coefficient u,v = Horizontal velocity components at each vertical level	X		X	
Turbulence Production Uittenbogaard (2003)	$$P_{veg} = \sqrt{\left(F_{d,veg,u} u\right)^2 + \left(F_{d,veg,v} v\right)^2}$$	X		X	
Turbulence Dissipation Uittenbogaard (2003)	$$D_{veg} = c_2 \frac{P_{veg}}{\tau_{eff}}$$ $$\tau_{eff} = min\,(\tau_{free}, \tau_{veg})$$ $$\tau_{free} = \frac{k}{\varepsilon}$$ $$\tau_{veg} = \left(\frac{L^2}{c_k{}^2 P_{veg}}\right)^{1/3}$$ $$L(z) = c_l \left(\frac{1 - b_v t_v n_v}{n_v}\right)^{1/2}$$ P_{veg} = Turbulence Production τ_{free} = Dissipation time scale of free turbulence k = Turbulent kinetic energy ε = Turbulence dissipation τ_{veg} = Dissipation time scale of free turbulence $$c_k = \left(c_\mu^0\right)^4 \simeq 0.09$$ L = typical length scale between the plants c_l = Lift coefficient of order unity	X		X	X

Wave Dissipation Mendez and Losada (2004) Dalrymple et al. (1984)	$$S_{d,veg} = \sqrt{\frac{2}{\pi}}\, g^2 \widetilde{C_D} b_v n_v \left(\frac{\tilde{k}}{\tilde{\sigma}}\right)^3$$ $$\frac{sinh^3(\tilde{k}l_v) + 3\,sinh(\tilde{k}l_v)}{3\tilde{k}cosh^3(\tilde{k}h)}\sqrt{E_{tot}}E(\sigma,\theta)$$ $\widetilde{C_D}$ = Bulk drag coefficient $\tilde{k}$ = Mean wave number $\tilde{\sigma}$ = Mean wave frequency h = Water depth E_{tot} = Total wave energy E = Wave energy at frequency σ and direction θ	X	X	X	
Wave induced streaming Luhar et al., 2010	$$F_{s,veg} = \frac{S_{d,veg,tot}}{\rho_0}\frac{\tilde{k}}{\tilde{\sigma}}$$ $S_{d,veg,tot}$ = Total wave energy dissipation $\tilde{k}$ = Mean wave number $\tilde{\sigma}$ = Mean wave frequency ρ_0 = Reference density of seawater	X	X	X	

Table 1: Processes in ROMS and SWAN to model the presence of vegetation. The different input parameters (stem density, n_v; height, l_v; diameter, b_v; and thickness, t_v) affecting model wave and hydrodynamics are included.

524
525
526
527
528
529
530
531
532

	Stem density (stems/m^2) n_v	Height (m) l_v	Diameter (mm) b_v	Thickness (mm) t_v
1.	144.3	0.24	6.0	0.6
2.	62.1	0.17	3.0	0.6
3.	226.5	0.3	6.0	0.3
4.	144.3	0.17	9.0	0.9
5.	144.3	0.3	3.0	0.9
6.	62.1	0.3	6.0	0.3
7.	226.5	0.17	6.0	0.3
8.	144.3	0.3	9.0	0.9
9.	144.3	0.24	9.0	0.3
10.	226.5	0.24	6.0	0.9
11.	144.3	0.24	3.0	0.3
12.	62.1	0.24	6.0	0.9
13.	62.1	0.17	6.0	0.3
14.	62.1	0.24	9.0	0.6
15.	144.3	0.17	3.0	0.9

533
534   **Table 2: Plant property input combination for different simulations during sensitivity analysis.**
535

538
539
540
541
542
543
544
545
546

	Plant Stem Density n_v	Plant Height l_v	Plant Diameter b_v	Plant Thickness t_v
Wave dissipation	0.68	0.24	0.032	0.01
Kinetic energy	0.36	0.44	0.12	0.03
Maximum water level change	0.38	0.43	0.15	0.01
Turbulent kinetic energy	0.35	0.42	0.12	0.03

547
548 **Table 3: Sobol Indices for all the outputs.**
549
550

551
552
553
554
555
556
557
558
559
560
561
562

563

564

565

566

567

568

569

570

571

572

573

574

575

- Depth-averaged horizontal velocity (U, V)
- Water level (h, η)

ROMS
flow model

SWAN
wave model

Wave parameters (H_s, λ, θ, T_t, T_b, U_b, S_d)

- Drag force ($F_{d,veg}$)
- Vertical turbulent mixing (P_{veg}, D_{veg})
- Wave-induced streaming ($F_{s,veg}$)

Vegetation parameters
(n_v, l_v, b_v, C_d)

Depth-varying horizontal velocity (u, v)

Wave dissipation ($S_{d,veg}$)
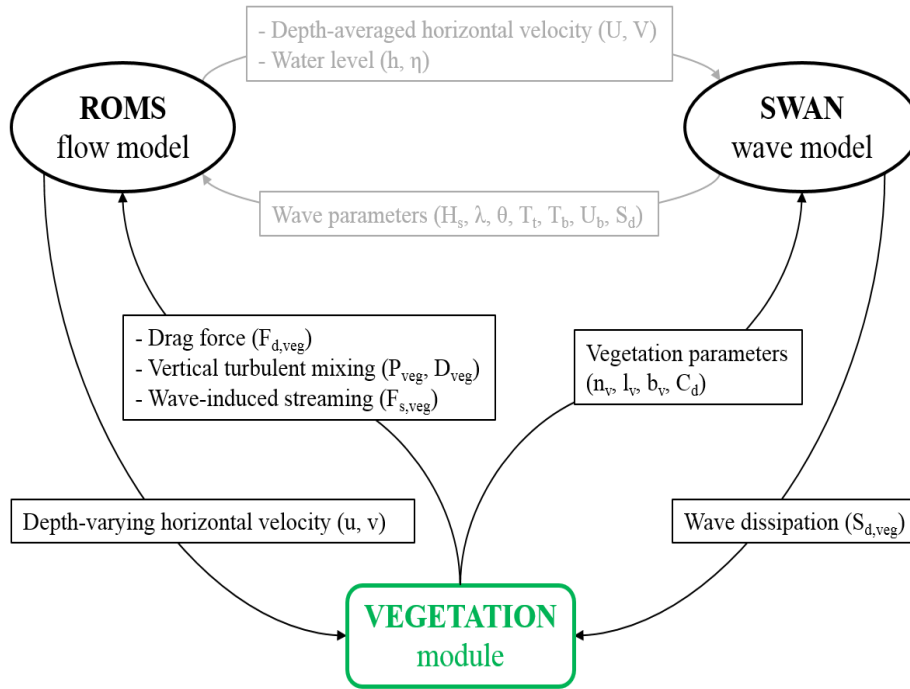
VEGETATION
module

Figure 1: Schematic showing the vegetation module implementation in COAWST model (Figure adapted from Beudin et. al, 2017)

578
579

580

9.2 km

Tidal amplitude =0.5 m
Tidal period = 12 hours

Wave height = 0.5 m
Wave period = 2 seconds
Wave direction = 0° (North)

y

x

z

1 km

9.8 km

1 km   Vegetation

z

y

x

Depth = 3 m

1 km

Vegetation
Height

9.8 km
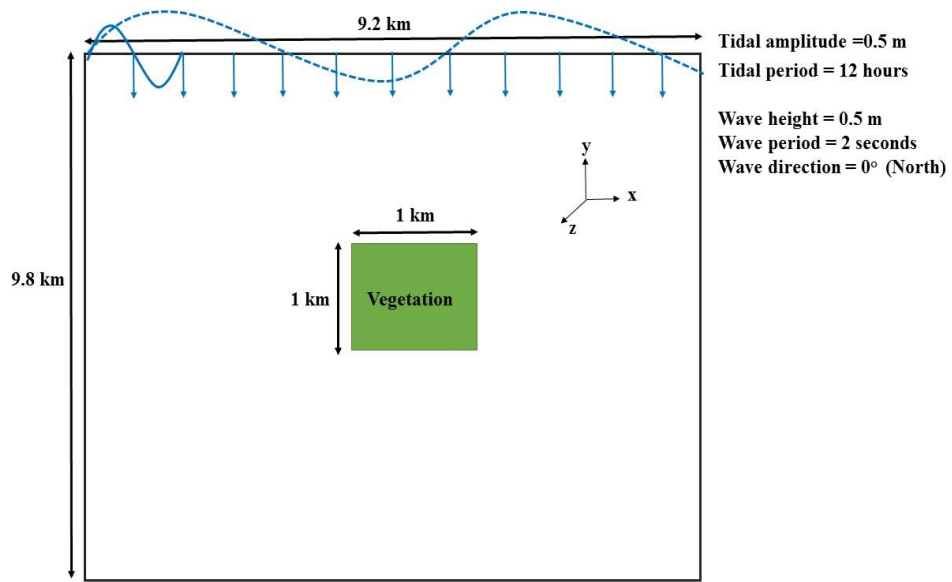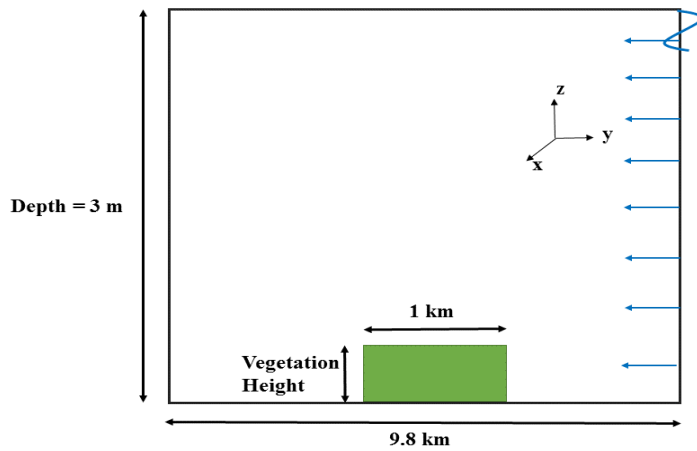
Figure 2: Schematic showing the idealized domain (Not drawn to scale)

(a) Plan view and (b) Cross-sectional view.
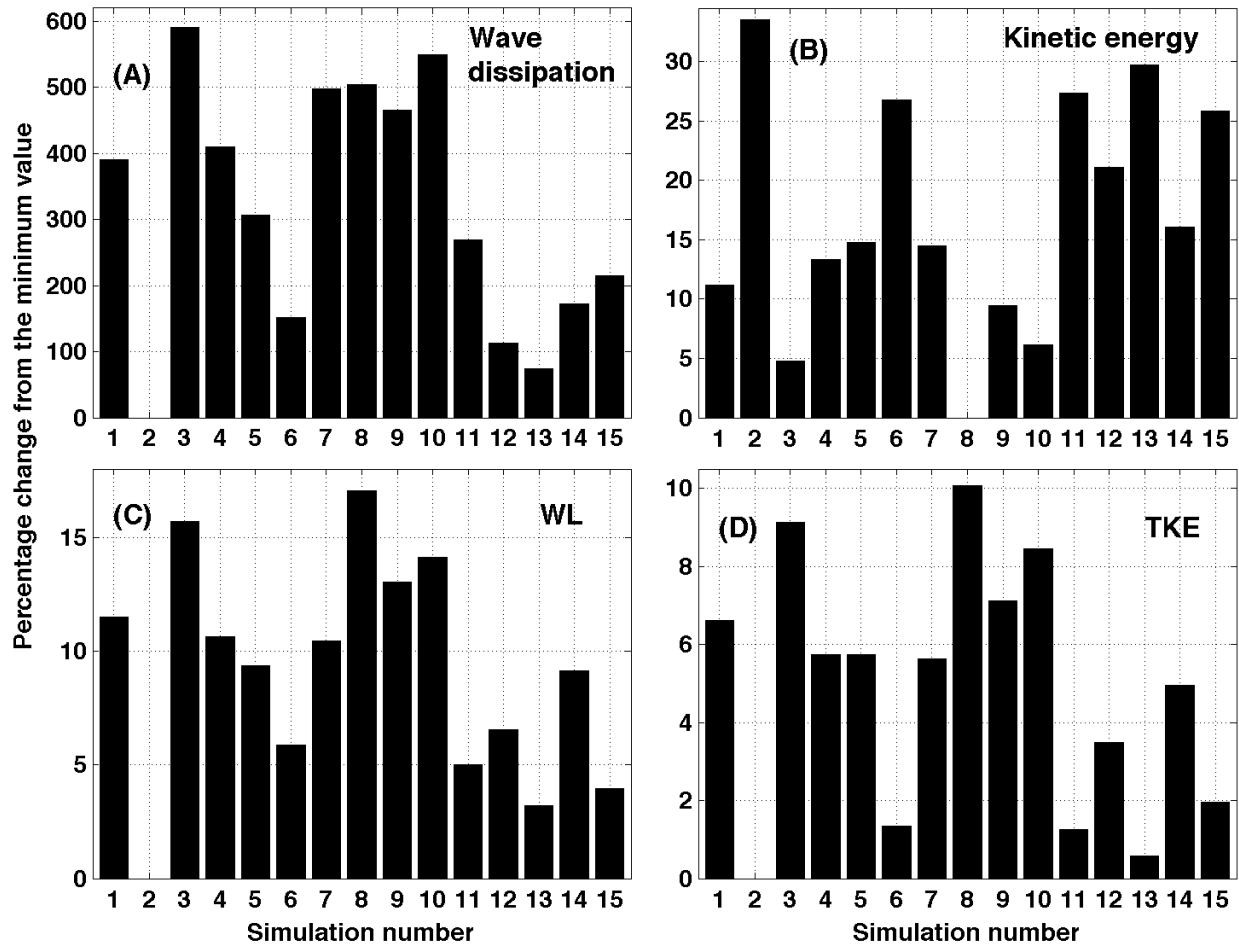
587
Figure 3: Percentage change from minimum for the four impact parameters: a) wave dissipation; b) kinetic energy; c) maximum water level change (WL); and d) Turbulent Kinetic Energy (TKE).

590
591
592
593
594
595
596
597
598
599
600
601
602
603
604
605
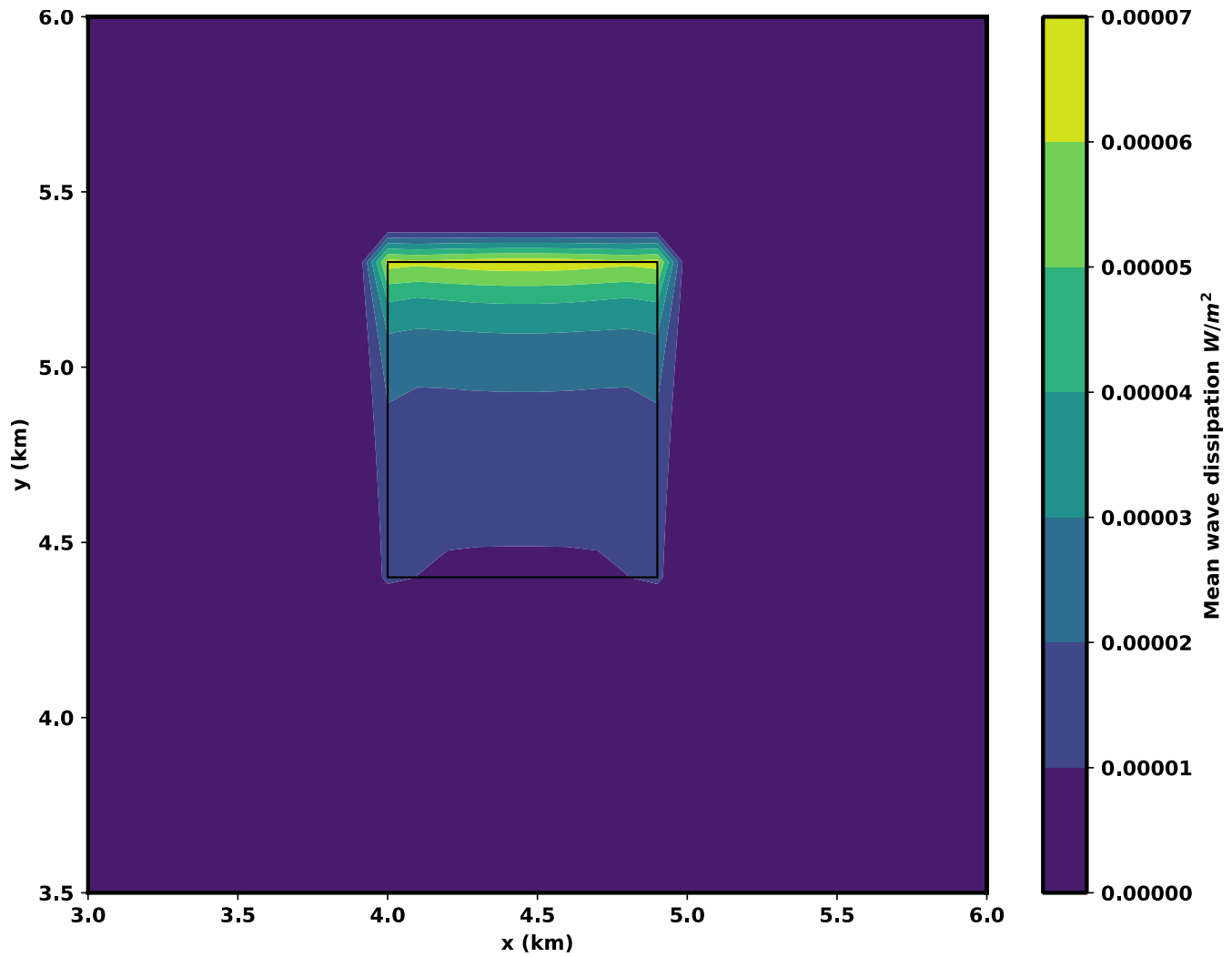
Figure 4: Standard deviation from wave dissipation (W m^{-2}) in presence of vegetation (Plan view). The area of the vegetation patch is highlighted in the middle of the domain.

611
612
613
614
615
616
617
618
619
620
621
622

626   **Figure 5: Standard deviation in kinetic energy (cm² s⁻¹) in presence of vegetation (cross-sectional view).**
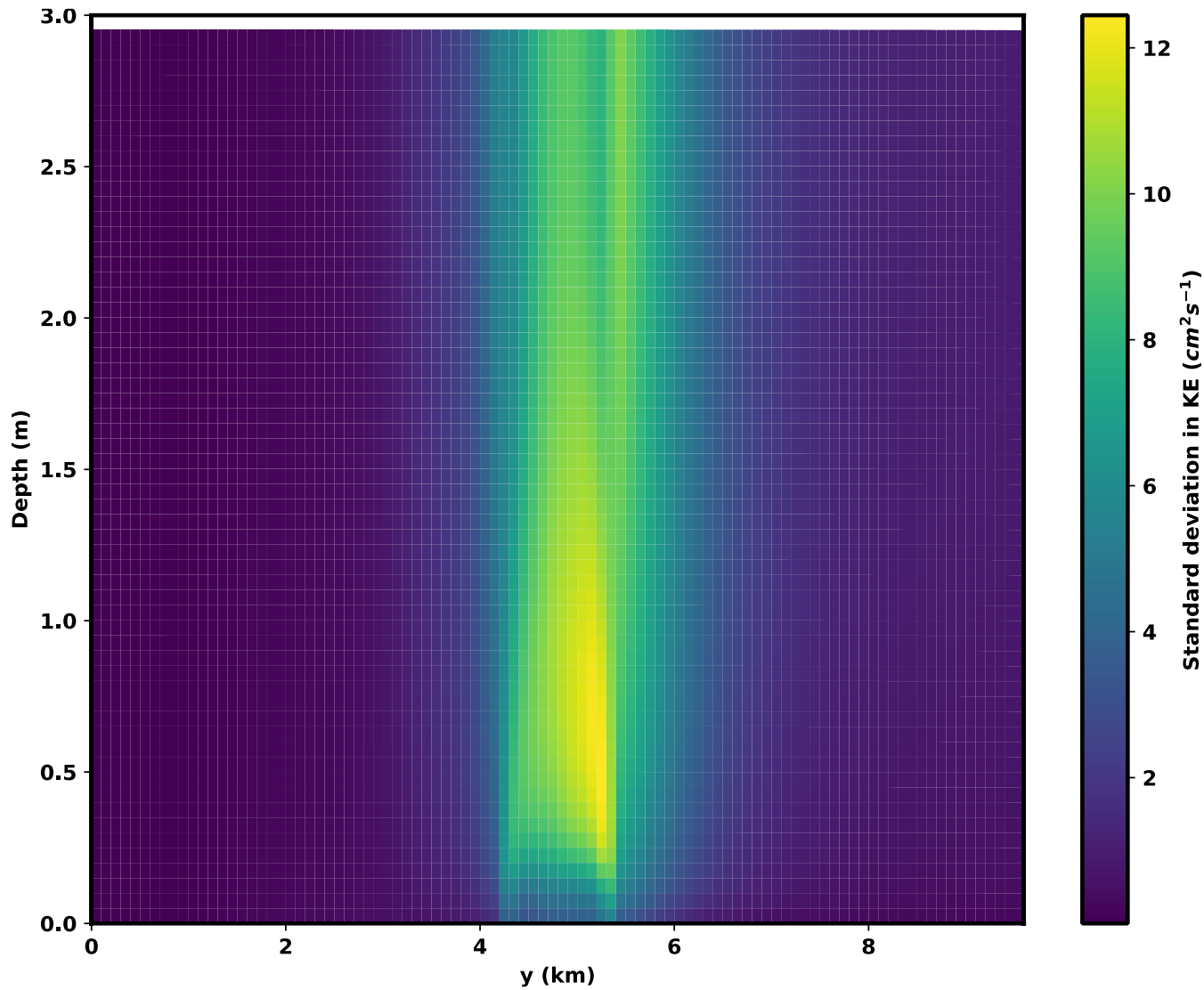
627
628
629
630
631
632
633
634
635
636
637
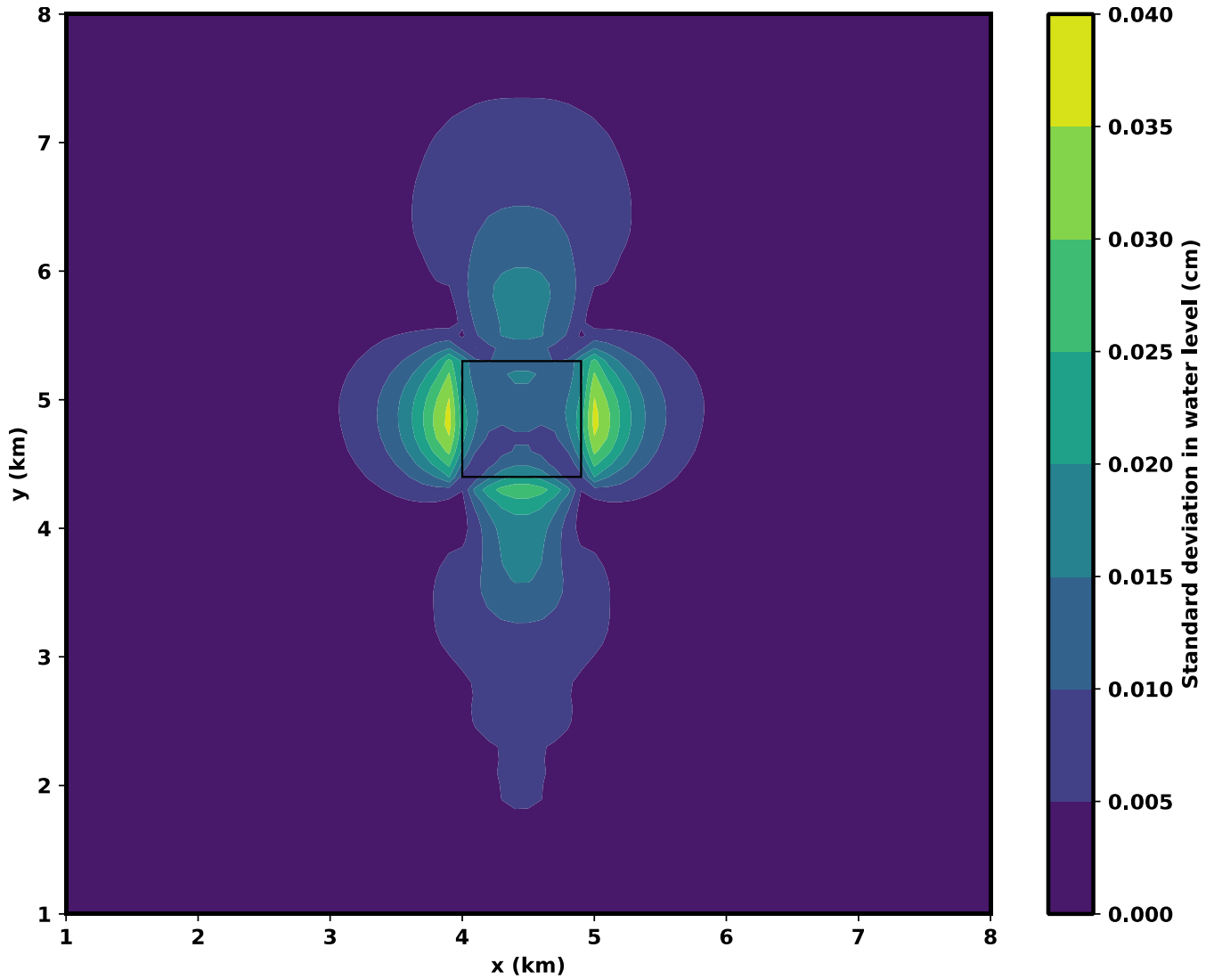
Figure 6: Standard deviation in water level in presence of vegetation (plan view). The area of the vegetation patch is highlighted in the middle of the domain.

25

654
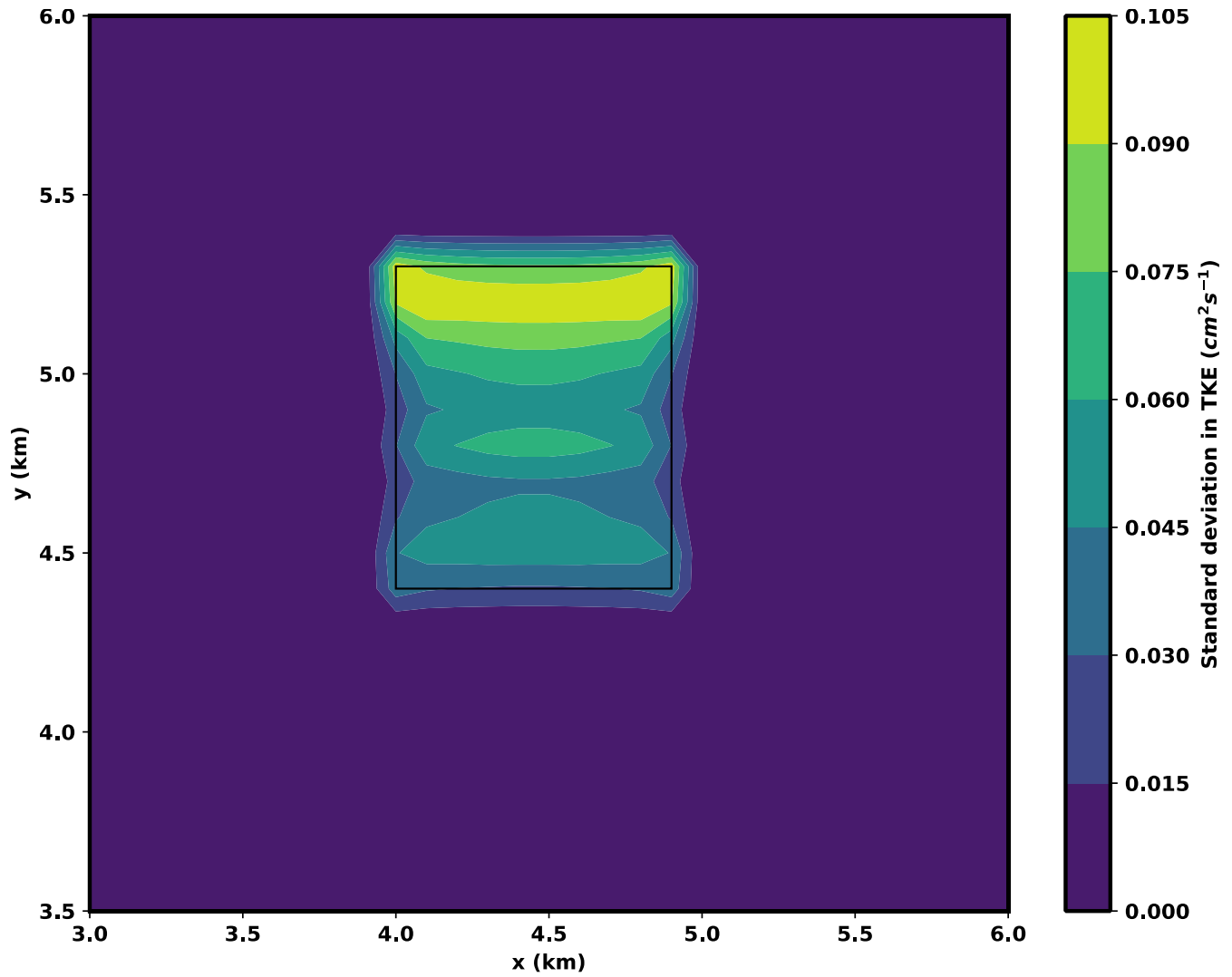
655
Figure 7: Standard deviation in Turbulent Kinetic Energy (TKE) (cm^2 s^{-1}) in presence of vegetation (plan view). The
area of the vegetation patch is highlighted in the middle of the domain.
658
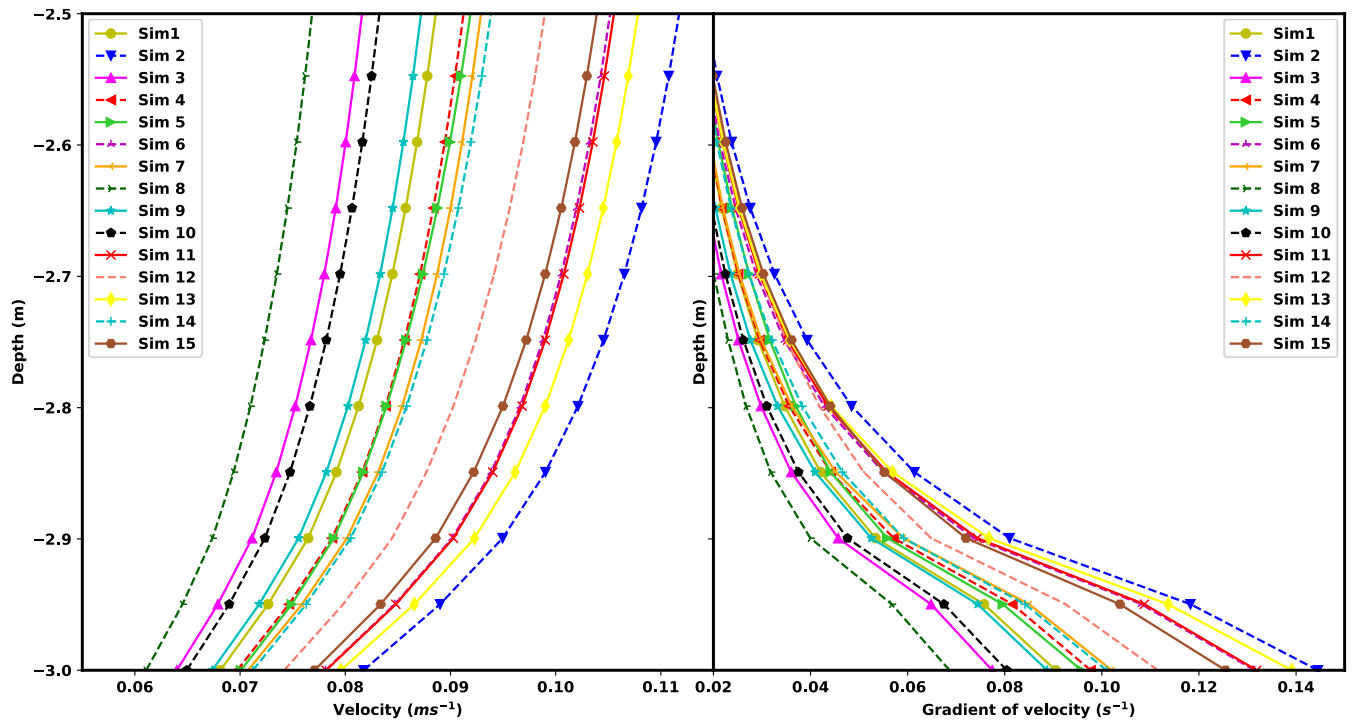
Figure 8: (a) Velocity (m s^{-1}) profile and (b) Vertical gradient (s[-1]) of velocity profile varying with depth in front of the vegetation patch at a particular time instance during flood for different simulations.